ACS APPLIED MATERIALS & INTERFACES

www.acsami.org

Research Article

High-Intensity Ultrasound-Assisted Low-Temperature Formulation of Lanthanum Zirconium Oxide Nanodispersion for Thin-Film Transistors

Pavan Pujar,[‖] Kishor Kumar Madaravalli Jagadeeshkumar,[‖] Muhammad Naqi,[‖] Srinivas Gandla, Hae Won Cho, Sung Hyeon Jung, Hyung Koun Cho, Jagannathan T. Kalathi,* and Sunkook Kim*

Cite This: https://dx.doi.org/10.1021/acsami.0c11193

Read Online

ACCESS | Metrics & More | Article Recommendations | Supporting Information

ABSTRACT: The process complexity, limited stability, and distinct synthesis and dispersion steps restrict the usage of multicomponent metal oxide nanodispersions in solution-processed electronics. Herein, sonochemistry is employed for the *in situ* synthesis and formulation of a colloidal nanodispersion of high-permittivity (κ) multicomponent lanthanum zirconium oxide (LZO: $La_2Zr_2O_7$). The continuous propagation of intense ultrasound waves in the aqueous medium allows the generation of oxidant species which, on reaction, form nanofragments of crystalline LZO at ~80 °C. Simultaneously, the presence of acidic byproducts in the vicinity promotes the formulation of a stable as-prepared LZO dispersion. The LZO thin film exhibits a κ of 16, and thin-film transistors (TFTs) based on LZO/indium gallium zinc oxide operate at low input voltages (≤4 V), with the maximum mobility (μ) and on/off ratio (I_{on}/I_{off}) of 5.45 ± 0.06 $cm^2\ V^{-1}\ s^{-1}$ and ~10^5, respectively. TFTs based on the compound dielectric LZO/Al_2O_3 present a marginal reduction in leakage current, along with enhancement in μ (6.16 ± 0.04 $cm^2\ V^{-1}\ s^{-1}$) and I_{on}/I_{off} (~10^5). Additionally, a 3 × 3 array of the proposed TFTs exhibits appreciable performance, with a μ of 3−6 $cm^2\ V^{-1}\ s^{-1}$, a threshold voltage of −0.5 to 0.8 V, a subthreshold swing of 0.3−0.6 V dec^{-1}, and an I_{on}/I_{off} of 1−2.5 (×10^6).

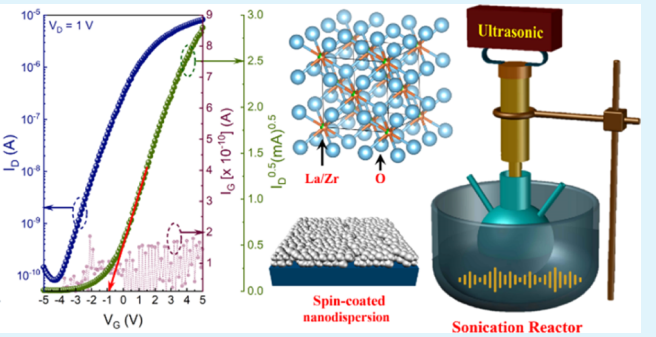

KEYWORDS: *dielectric, LZO, low temperature, sonochemical, nanodispersions, IGZO*

1. INTRODUCTION

The remarkable progress in the solution processing of functional thin films for large-area, flexible electronics has offered numerous opportunities for the development of advanced materials and innovative routes for thin-film deposition. Solution processing is a low-cost and simple alternative, wherein a precursor loaded with the material of interest is utilized in the deposition of a thin film using comparatively less capital-intensive equipment such as a spin coater, spray coater, and inkjet printer.[1,2] Unlike high-vacuum conventional vapor phase deposition routes, solution processing facilitates the deposition of thin films at ambient pressure with minimum complexity.[1,3] Thin films of various classes of functional materials such as metal oxides, organic molecules, two-dimensional (2D) materials, metal nanoparticles, and carbon nanotubes have been deposited *via* solution processing using two distinct strategies.[1] In the first, nanoparticle dispersions (NPDs), that is, nanofragments of the functional material, are dispersed in solvent(s) with appropriate dispersants and/or surface-active agents.[3,4] The surface-active agents allow the nanofragments to form a stable as-prepared colloidal dispersion and mitigate undesirable agglomeration. In the second, soluble chemical precursors (SCPs), where the starting materials, for instance, metal salts (in the case of functional metal oxides), are dissolved in a solvent medium with appropriate stabilizers and other additives.[3,5,6] NPDs are advantageous for low-temperature processing because of the presence of the presynthesized nanomaterial. However, they present a series of drawbacks such as compromised film densification, difficulty in processing multicomponent functional metal oxides, numerous processing steps, limited stability, and moderate temperature required to ensure that the thin films are free from surface-active agents. On the other hand, SCPs require high-processing temperatures for the *in situ* formation and densification of the deposited material.[5,7] Over the years, a series of modifications such as chelate routes in sol−gel,[8,9] metal−organic decomposition,[9] sol−gel on chip,[10]

Received: June 19, 2020
Accepted: September 8, 2020
Published: September 8, 2020

combustion processing,[11,12] photochemical activation,[13] aqueous processing,[14,15] microemulsions,[16] and polymer-assisted depositions[17,18] in SCPs have been proposed to lower the processing temperature and fabricate electrically robust thin films. Despite the aforementioned drawbacks of NPDs, the large surface area of nanoparticles renders them efficient for use in the fabrication of charge-transporting layers in solar cells and light-emitting diodes.[19] Therefore, it is essential to overcome the limitations of NPDs and utilize their scientific and technological potential. In this regard, the present work is aimed at the *in situ* formulation of a multicomponent functional metal oxide dispersion through an untapped energy source—high-intensity ultrasound. The utilization of ultrasound energy for chemical reactions and processes constitutes the "sonochemical" method. This greener and inherently safer approach enables the effortless, *in situ* formulation of a nanodispersion and bypasses the separate substeps of synthesis and dispersion.

The sonochemical method enables the use of microscopic supercritical conditions, such as high temperatures and liquid pressures, that are often not easily obtained by other conventional methods such as hydrothermal, sol–gel, and solution combustion.[20] Shock waves and local turbulence are created by acoustic cavitation at the microscopic level during the ultrasonic irradiation of liquids.[21] Acoustic cavitation is the continuous creation, growth, and implosive collapse of microbubbles in liquids. During cavitation, the collapse of microbubbles causes intense localized heating (temperature ~ 1000 K) and a high pressure of 10^7 Pa for relatively short timescales.[22] The microbubble behaves as a tiny microreactor during its collapse, which generates heat and produces unique reactive species such as $OH^•$ and $H^•$ radicals. Hence, high-energy chemical reactions, improved mixing, and enhanced heat- and mass-transfer rates can be obtained by the sonochemical method. Consequently, it is directly employed for the *in situ* synthesis and formulation of NPDs of multicomponent functional metal oxides. The present study is the first report demonstrating the efficacy of the sonochemical method in the formulation of a nanodispersion of a high-κ dielectric, lanthanum zirconium oxide (LZO: $La_2Zr_2O_7$).[23] Among the various high-κ materials (La_2O_3, ZrO_2, Ta_2O_5, Al_2O_3, and Li_2O),[24,25] La_2O_3 possesses a high κ of 27. However, the hygroscopic nature of La_2O_3 promotes the formation of undesired lanthanum hydroxide [$La(OH)_3$], which is addressed by the addition of zirconium (La/Zr: 1:1);[23] Figure S1 shows the position of LZO on a composition–temperature plane of La_2O_3–ZrO_2.[26] The LZO nanodispersion was used for the fabrication of high-κ thin films, which were useful in the low-voltage operation of indium gallium zinc oxide (IGZO) thin-film transistors (TFTs). In addition, integration of the same with Al_2O_3 (10 nm), grown by atomic layer deposition (ALD), was conducted to understand the effect of the compound LZO/Al_2O_3 dielectric on the performance of IGZO TFTs.

2. EXPERIMENTAL SECTION

2.1. Formulation of LZO Dispersion and Synthesis of Nanopowder. All reagents were purchased from Sigma-Aldrich and used without further purification. Lanthanum chloride ($LaCl_3$) and zirconium oxynitrate ($ZrO(NO_3)_2$) were used as starting materials. Both reagents were dissolved in deionized water separately, then mixed in a round-bottomed flask, and vigorously stirred for 15 min at room temperature. The precursor solution was sonicated for 30 min at 50% amplitude of a 500 W power supply, using a 20 kHz probe sonicator. Sonication was conducted in the pulse mode (4 s ON and 2 s OFF) at a constant temperature using a controlled cooling bath; the maximum temperature attained during the sonochemical reaction was measured to be 80 °C. After intense sonication for an optimized time span of 30 min, the colloidal dispersion was obtained. The resulting nanodispersion was used in two distinct ways: first, a small volume fraction of the LZO nanodispersion was dried in a hot-air oven (100 °C for 24 h); second, the remaining fraction was further utilized for film fabrication.

2.2. Characterization of LZO Dispersion and Nanopowder. The diluted LZO dispersion was analyzed using a particle size analyzer (HORIBA SZ-100) and a transmission electron microscope (JEM-2100, JEOL; operating voltage: 200 kV) to estimate the size distribution of nanoparticles and quantify the *d*-spacing from the high-resolution LZO fringe pattern. The phase purity and crystal structure of the synthesized LZO powder were determined from powder X-ray diffraction (XRD) (Bruker D8 DISCOVER diffractometer) using Cu Kα radiation (λ = 0.15406 nm), with a step size of 0.04° and a scan rate of 2° min^{-1}. Rietveld analysis of the obtained diffraction pattern was then performed using the FullProf Suite, and the three-dimensional (3D) view of the crystal structure was generated using the VESTA visual interface. The chemical composition of the synthesized LZO nanopowder was analyzed by X-ray photoelectron spectroscopy (XPS) (ESCA 2000 MultiLab 2000). The binding energy scale was in electron volts (eV), and the high-resolution spectrum of carbon 1s (position: 284.7 eV) was used for internal calibration. The peak-fit analysis of the spectrum was performed using the CASAXPS 2.3.22PR1.0 software package.

2.3. Deposition and Characterization of Thin Films. The LZO dispersion was spin-coated (3000 rpm, 30 s, ramp up: 20 s) onto a solvent-cleaned, oxygen plasma-treated (power: 60 W, for 60 s), and heavily doped silicon substrate. The as-spun film was annealed at 350 °C followed by slow cooling. This process was repeated twice to obtain the desired thickness. The surface morphology of the spin-coated LZO thin films was observed by field-emission scanning electron microscopy (FESEM; JSM-6700F, Hitachi) in conjunction with energy-dispersive spectroscopic mapping of lanthanum, zirconium, and oxygen.

2.4. Fabrication and Characterization of TFTs. The LZO thin films were utilized for the fabrication of TFTs; two sets of devices were fabricated using the LZO and LZO/Al_2O_3 dielectrics. The areal capacitance of the dielectrics was estimated using the metal–insulator–metal (MIM) architecture. For TFTs based on the LZO/Al_2O_3 dielectric, an additional 10 nm Al_2O_3 was grown on the LZO thin film by ALD (Lucida D100, NCD Co., Ltd.). Furthermore, semiconducting amorphous IGZO thin films (In/Ga/Zn atomic ratio: 2:1:2 and thickness: 30 nm) were deposited onto the LZO and LZO/Al_2O_3 layers *via* radio-frequency (RF) sputtering at room temperature and then patterned by conventional photolithography, in which the photoresist (PR, AZGXR-601, MERCK) was spin-coated onto the top surface for 20 s at 3000 rpm. Subsequently, the unwanted area of amorphous IGZO was etched using a diluted buffer oxide etchant for 10 s and cleaned with acetone. The pattered IGZO channel was then annealed for 1 h at 300 °C. To pattern the top contacts, the lift-off process was employed, in which the lift-off resist (Product #G367070500L1GL, MicroChem) was spin-coated for 45 s at 2000 rpm and annealed at 180 °C for 5 min; following this, the PR was spin-coated for 20 s at 3000 rpm and annealed at 90 °C for 2 min. The patterns of the top contacts were then developed using a developer (AZ-300MIF) after UV exposure in the presence of a patterned mask. Finally, the top contact metals (Ti/Au ~ 20/100 nm) were deposited using an e-beam evaporator, and the unwanted area was removed using a PG remover (mr-Rem 700, Micro Resist Technology). The electrical characteristics of the fabricated devices were estimated using a semiconductor parameter analyzer (SCS-4200A, Keithley).

https://dx.doi.org/10.1021/acsami.0c11193
ACS Appl. Mater. Interfaces XXXX, XXX, XXX–XXX

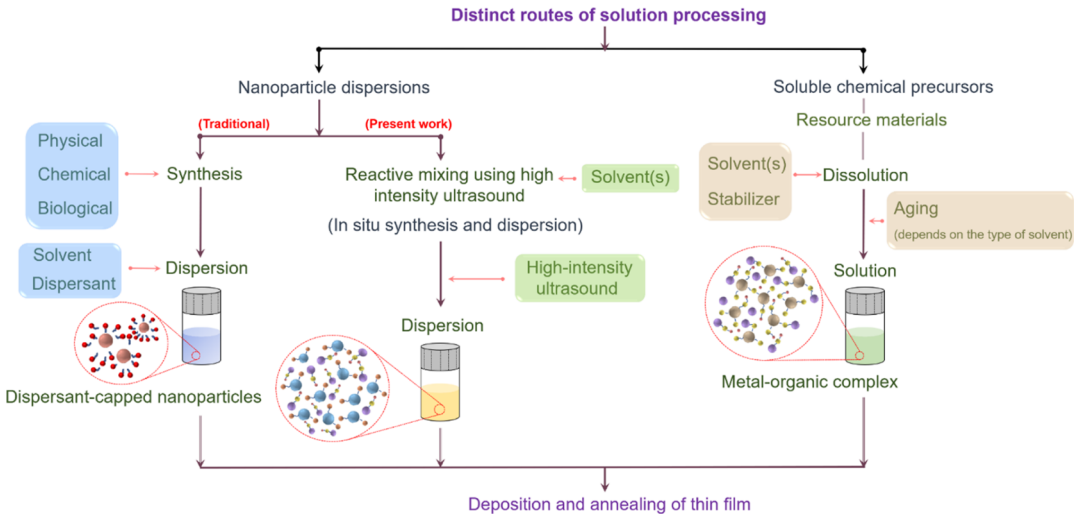

Figure 1. Distinct routes of solution processing: this chart compares the different routes (present work and the literature) of solution processing. The traditional route using NPDs requires an additional synthesis step, whereas the sonochemical method enables *in situ* synthesis and dispersion at low temperatures. On the other hand, SCPs do not use presynthesized nanomaterials.

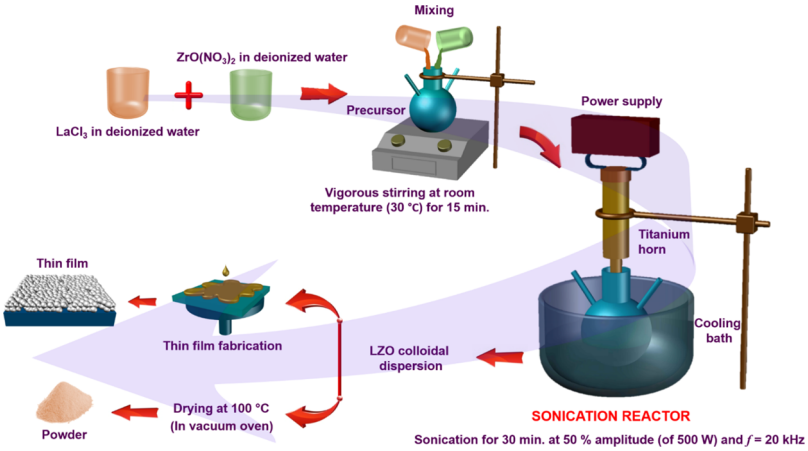

Figure 2. Sonochemical method: this schematic presents the stepwise procedure for the formulation of a LZO nanodispersion and its derived products (bulk powder and thin film).

3. RESULTS AND DISCUSSION

The sonochemical method is proposed as a new and simple route for the direct formulation of complex multicomponent functional metal oxide nanodispersions. A comparison of existing solution-processing routes and the sonochemical method is presented in Figure 1 and Table S1. The ultrasound-based sonochemical method is comparatively less cumbersome than the traditional route. The utilization of ultrasound energy is widely being explored for the liquid exfoliation (LE) of layered materials.[27] In LE, ultrasound allows the separation of 2D layers from the bulk material, promoting the formation of colloidal dispersions of exfoliated layers. The present sonochemical method goes beyond LE, where ultrasound energy is utilized for the *in situ* synthesis and formulation of nanodispersions and is not limited to only layered materials. The initial aqueous precursor, composed of sources of lanthanum and zirconium, is subjected to high-intensity sonication (f = 20 kHz) in an ambient atmosphere. During sonication, the acoustic waves propagate by pressure oscillation within the liquid medium.

When the amplitude of an acoustic wave pressure exceeds the ambient pressure, the instantaneous pressure becomes negative during the rarefaction of waves.[28] The negative pressure is defined as the force acting on the surface of the liquid element per unit surface area. The negative instantaneous local pressure results in the creation of a mist of microbubbles.[29] The continuous action of ultrasound of a fixed frequency leads to the collapse of microbubbles within nanoseconds. During this collapse stage, the temperature and pressure inside the bubbles rise to thousands of Kelvin and thousands of bars, respectively.[30] As a result, water vapor and oxygen undergo dissociation inside the microbubble, resulting in the formation of oxidants such as OH and H_2O_2. These reactive oxidant species dissolve gradually and aid in the formation of the required metal oxides through a systematic reaction with the precursors.[31] Eqs 1−3 describe the chemical reactions involved in the sonochemical synthesis of LZO. The oxidant reactive species (H_2O_2 and H_2), resulting from the sonolytic dissociation of water vapor, further react with $LaCl_3$ and $ZrO(NO_3)_2$ to form $La_2Zr_2O_7$ (eq 3).

https://dx.doi.org/10.1021/acsami.0c11193
ACS Appl. Mater. Interfaces XXXX, XXX, XXX−XXX

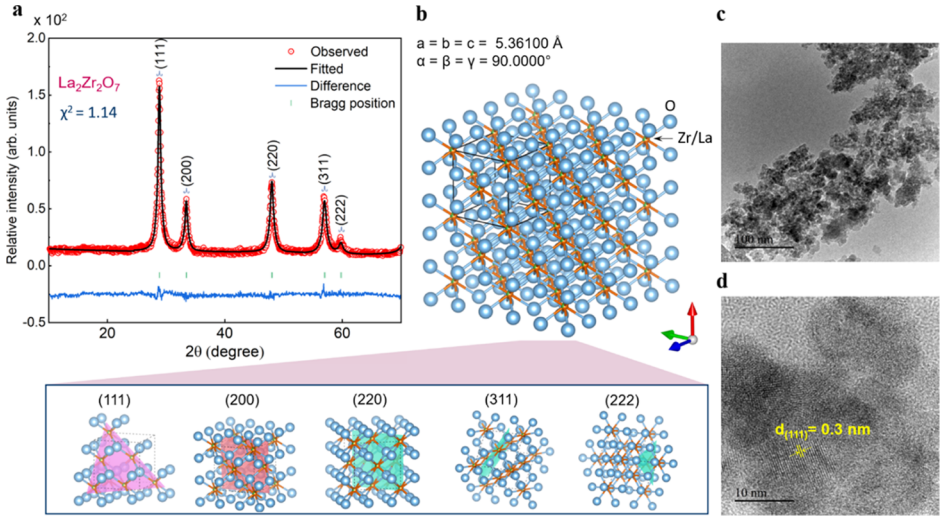

Figure 3. Structural and morphological analysis of LZO powder: (a) Rietveld-refined XRD pattern of LZO. (b) 3D crystal structure produced from refined XRD data along with diffraction planes. Transmission electron micrographs of (c) LZO particles and (d) high-resolution fringe pattern.

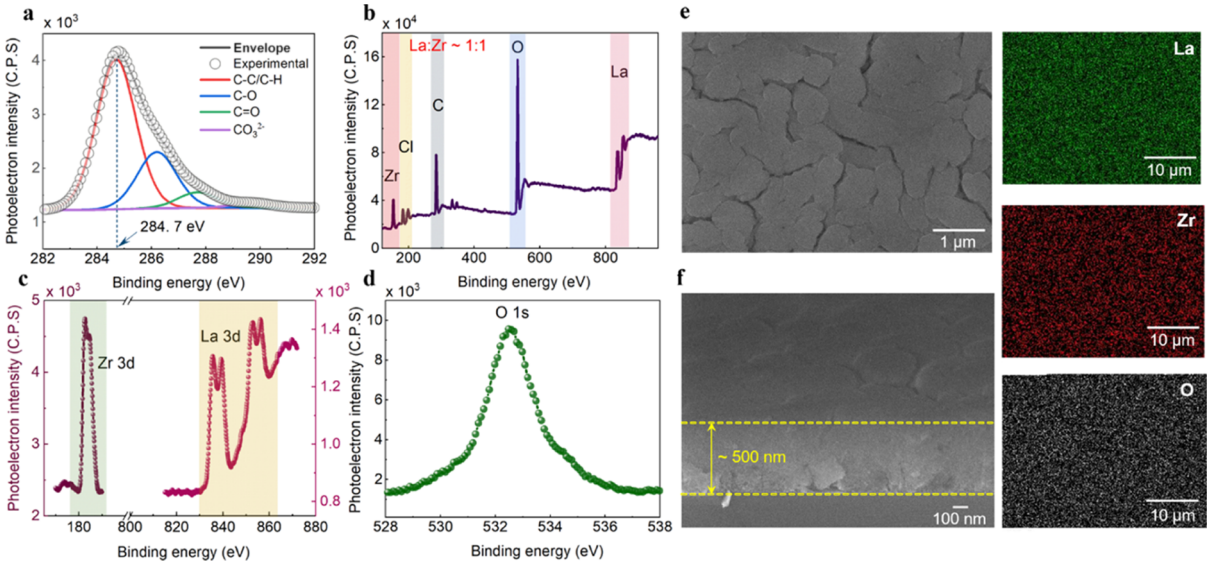

Figure 4. Chemical composition analysis by XPS: (a) C 1s peak positioned at 284.7 eV, (b) low-resolution survey spectrum and high-resolution spectra of (c) Zr 3d, La 3d, and (d) O 1s. Morphology and elemental distribution of the LZO surface: (e) field-emission scanning electron micrograph depicting the sintered particles of LZO and the distribution of lanthanum, zirconium, and oxygen; (f) cross-sectional micrograph of the LZO thin film presenting its thickness.

$$\left.\begin{aligned} &H_2O \rightarrow H^\bullet + OH^\bullet \\ &H^\bullet + H^\bullet \rightarrow H_2 \\ &OH^\bullet + OH^\bullet \rightarrow H_2O_2 \end{aligned}\right\}$$

formation of reactive species under the action of ultrasound (1)

$$\left.\begin{aligned} &NO_3 \rightarrow O + NO_2 \\ &NO_2 + OH^\bullet \rightarrow HNO_3 \end{aligned}\right\}\text{formation of byproducts} \quad (2)$$

$$2LaCl_3 + 2[ZrO(NO_3)_2H_2O] + 3H_2O \xrightarrow[\text{sonication}]{H_2O_2\ \&\ H_2} La_2Zr_2O_7 + 6HCl + 4HNO_3 \quad (3)$$

It is interesting to note that the byproducts of the reaction, namely, HCl and HNO_3, make the resultant colloidal solution of LZO acidic. The measured pH levels of the precursor and the product (LZO nanodispersion) were found to be 7.2 (near-neutral) and 5.3 (acidic), respectively. The product (LZO) is in the form of a uniformly distributed secondary phase of nanoparticles in an acidic liquid medium. The chlorine ions of HCl act as ligands attached to the LZO particle surface, allowing it to disperse uniformly without agglomeration.[32] The LZO nanoparticles in the solution exhibit sizes in the range of 30−50 nm (Figure S2). Along with the narrow size distribution, the LZO nanoparticles are of uniform shape, which is attributed to the creation of uniform-sized microbubbles that act as nanoreactors. The obtained LZO dispersion can further be used to obtain the bulk nanopowder and thin films on a substrate of interest. The stepwise process with the end products of the sonochemical reaction is presented in Figure 2.

https://dx.doi.org/10.1021/acsami.0c11193
ACS Appl. Mater. Interfaces XXXX, XXX, XXX−XXX

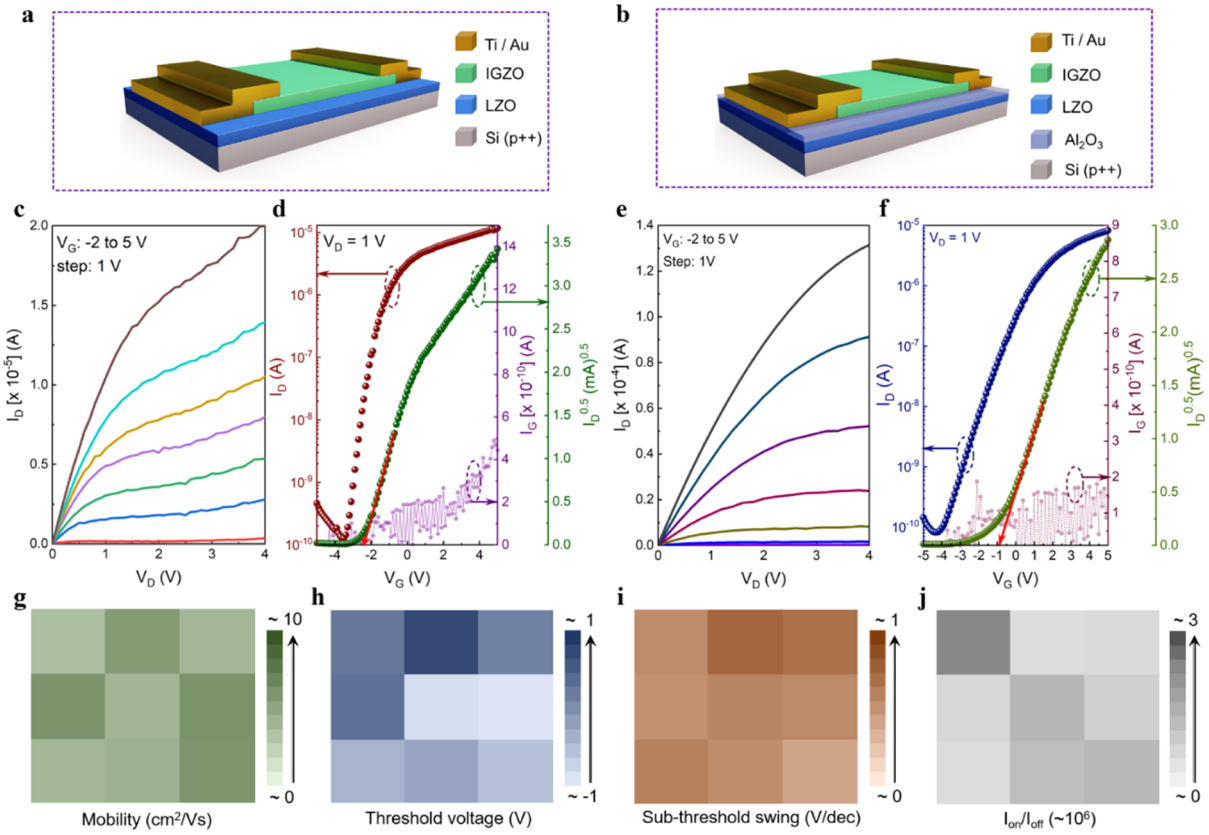

Figure 5. Electrical characteristics of the proposed TFT. (a,b) 3D section view of proposed TFTs composed of LZO and LZO/Al_2O_3 dielectric layers, respectively. (c) Output graph of the LZO dielectric thin-film-based TFT device at different gate-bias (V_G) ranges from −2 to 5 V with a step of 1 V. (d) Transfer curve of the LZO dielectric thin-film-based TFT device at a V_D of 1 V. (e,f) Output and transfer properties of the LZO/Al_2O_3 dielectric thin-film-based TFT device under the same conditions as those of the LZO dielectric thin-film-based TFT device. Mapping representation of a 3 × 3 transistor array in terms of (g) mobility ($cm^2\ V^{-1}\ s^{-1}$), (h) threshold voltage (V), (i) sub-threshold swing (V dec^{-1}), and (j) I_{on}/I_{off}.

The LZO nanodispersion was first used to obtain a nanopowder by simple drying under flowing hot air at 100 °C for 24 h. The resulting nanopowder was analyzed by XRD to understand the structural nature of LZO (Figure 3a). The Rietveld-refined XRD pattern reveals highly crystalline and phase-pure LZO. Notably, the maximum temperature used to obtain high crystallinity did not exceed 100 °C, and no further calcination was necessary. The unique reaction phenomena, such as the intensive collapse of the microbubbles leading to the formation of reactive oxidant species, enable the realization of low-temperature crystallinity.[33] The refined XRD pattern was used to predict the crystal structure and diffraction planes (Figure 3b). The diffraction peaks can be assigned to those of the cubic fluorite structure (space group: $Fm\bar{3}m$) of LZO with lattice parameters a = 5.361 Å ($=b = c$) and α = 90° ($=\beta = \gamma$). The average crystallite size of the LZO particles was estimated from the Scherrer relationship for all peaks to be 13.78 ± 1.7 nm. Subsequently, the diluted nanodispersion was allowed to dry on a transmission electron microscope copper grid for microstructure analysis. Figure 3c,d shows low- and high-resolution micrographs of the LZO nanoparticles, with a measured fringe distance of 0.3 nm—well matching with the XRD results. The chemical composition of the LZO powder was then analyzed by XPS.

The spectra of LZO were calibrated using the carbon 1s (C 1s) spectrum positioned at 284.7 eV (Figure 4a). The presence of lanthanum and zirconium in the 1:1 ratio is clear from the low-resolution survey spectrum (Figure 4b). For internal consistency of the data, high-resolution spectra of La 3d, Zr 3d, and O 1s are presented in Figure 4c,d. From these observations, it is confirmed that the synthesized nanopowder of LZO possesses a single-phase fluorite structure with the expected equimolar chemical composition. Furthermore, the LZO nanodispersion was used to fabricate thin films *via* spin coating. The thin films of LZO exhibit a continuous, uniform, and dense morphology, with a thickness of approximately 500 nm (Figure 4e,f). The compactness of the LZO film, without any localized sintered clusters of nanoparticles, represents the coatable standard of the nanodispersion. A dense morphology of functional metal oxide films is essential for robust electrical properties. The surface scanning electron micrograph of the LZO film confirms uniform sintering of the nanoparticles, with no trace of secondary, morphologically distinct impurities. Moreover, the distribution of lanthanum, zirconium, and oxygen on the surface of LZO confirms the compositional uniformity.

Subsequently, a MIM capacitor with LZO as an insulating layer was used to understand the dielectric response of LZO. Figure S3 shows the $C-V$ response of the capacitor with a dielectric κ of 16. The TFTs composed of the LZO dielectric and a RF-sputtered n-type amorphous IGZO semiconductor were also characterized under ambient conditions. In addition, the root mean square roughness of IGZO was obtained to be 0.717 nm, elaborating a smooth surface as shown in Figure S4.

https://dx.doi.org/10.1021/acsami.0c11193
ACS Appl. Mater. Interfaces XXXX, XXX, XXX−XXX

Alternatively, a compound dielectric approach was utilized for the fabrication of TFTs—a capping layer of 10 nm ALD-grown Al_2O_3 on LZO was integrated with amorphous IGZO. The architectures of the TFTs are shown in Figure 5a,b. A low current saturation at a high drain voltage (V_D) with linear behavior at low V_D was observed in the output plot in different gate-voltage (V_G) ranges from −2 to 5 V with a 1 V step (Figure 5c). Figure 5d shows the transfer curve of the LZO-based TFT in the log-linear scale with the leakage current (I_G); it exhibits an I_{on}/I_{off} on the order of ∼10^5 at a V_D of 1 V, a threshold voltage (V_T) of −2.1 V, and maximum I_G on the order of 5 × 10^{-10} A. Moreover, the maximum field-effect mobility (μ) of 5.45 ± 0.06 $cm^2\ V^{-1}\ s^{-1}$ was estimated from the mathematical relation $\mu = 2LI_D/WC_{ox}(V_G - V_T)^2$, where the channel length (L) and width (W) were maintained as 7 and 20 μm, respectively. To compare the performance characteristics of TFTs based on the LZO dielectric and the compound (LZO/Al_2O_3) dielectric, the performance of the LZO/Al_2O_3-based TFTs was measured. A high saturation current at a high V_D, with linear behavior at a low V_D, was observed in the output curve (Figure 5e) at different V_G bias ranges from −2 to 5 V with a 1 V step. Figure 5f presents the transfer curve of the LZO/Al_2O_3-based TFT, showing I_{on}/I_{off} ∼ 10^5 (at V_D = 1 V), V_T of −0.95 V, and I_G on the order of 1.5 × 10^{-10} A. Before estimating μ, the areal capacitance of the compound dielectric was measured. Figure S5 presents the C–V response of LZO/Al_2O_3. The maximum μ of 6.16 ± 0.04 $cm^2\ V^{-1}\ s^{-1}$ was estimated from the previously presented relation. These static performance parameters clearly illustrate the enhancement in the performance of TFTs based on the LZO/Al_2O_3 compound dielectric. Furthermore, the performance of the TFTs is compared with the previous reports (Table S2). Notably, the polycrystalline LZO, when deposited from its nanodispersion, may cause leakage due to the presence of deteriorating grain boundaries. Hence, the additional amorphous and dense capping layer of Al_2O_3 blocks the current to a certain extent, thereby reducing I_G. Furthermore, the hysteresis of the proposed device is measured and a minor difference of a threshold voltage (ΔV_T) of 0.27 V was observed with respect to the forward and reverse biases, as shown in Figure S6. To analyze the time stability of the proposed TFTs, the TFTs were stored in an ambient atmosphere for 45 days and then characterized. The transfer curve after 45 days found to shift toward a lower threshold voltage (Figure S7), which may be due to the lack of protection from the interaction between the channel material and the outer environment.

Furthermore, the improved marginal properties of LZO/Al_2O_3-based TFTs over LZO-based TFTs, a 3 × 3 transistor array based on the LZO/Al_2O_3 dielectric layer was fabricated to analyze the transistor performance over a large area. The performance of the transistor array was defined in terms of μ, V_T, sub-threshold swing (SS ∼ V dec^{-1}), and I_{on}/I_{off}, which were within the range of 3–6 $cm^2\ V^{-1}\ s^{-1}$, −0.5 to 0.8, 0.3–0.6 V dec^{-1}, and 1–2.5 (×10^6), respectively, as shown in Figure 5g–j. The performance parameters of the TFTs indicate their reliable behavior over a large scale, thus providing a new platform for next-generation electronic applications.

4. CONCLUSIONS

The present work demonstrates the *in situ* synthesis and formulation of a nanodispersion of a high-κ dielectric, LZO. Both the synthesis and formulation of the nanodispersion were achieved by the sonochemical method. This method utilizes high-intensity ultrasound waves in an aqueous medium; the continuous propagation of ultrasound waves leads to the formation of highly reactive oxidant species, which on reaction with metal salts forms metal oxide nanocrystals. The reaction temperature of 80 °C was sufficient to prepare polycrystalline LZO with a cubic fluorite structure. The calcination-free approach in the development of highly crystalline LZO without secondary impure phases makes the sonochemical method a more economical and greener alternative. The LZO nanodispersion was utilized to obtain a bulk nanopowder and a compositionally robust film. The LZO film presented a dielectric κ of 16. The TFTs based on LZO/IGZO and LZO/Al_2O_3/IGZO exhibited a distinctly improved performance, with a maximum μ and an I_{on}/I_{off} of 6.16 $cm^2\ V^{-1}\ s^{-1}$ and ∼10^5, respectively, along with minor hysteresis (27 V) and good stability over a time span of 45 days. These results trigger a new route of solution-processed metal oxide thin films with multiple advantages such as aqueous processing, low-temperature *in situ* synthesis, and dispersion. The present work is the first report on the performance of TFTs with sonochemical-derived multicomponent LZO dielectric for next-generation large-area electronics.

■ ASSOCIATED CONTENT

Supporting Information

The Supporting Information is available free of charge at https://pubs.acs.org/doi/10.1021/acsami.0c11193.

Comparison between solution-processing routes and the present sonochemical route; binary phase diagram of La_2O_3–ZrO_2; size distribution of LZO nanodispersion; areal capacitance of LZO; atomic force microscopy surface topography of the IGZO thin film; areal capacitance of the LZO/Al_2O_3 dielectric; and hysteresis and aging effect of the LZO/Al_2O_3-based IGZO TFT (PDF)

■ AUTHOR INFORMATION

Corresponding Authors

Jagannathan T. Kalathi − *Soft Materials Research Lab, Department of Chemical Engineering, National Institute of Technology Karnataka, Surathkal, India*; Email: jag@nitk.ac.in

Sunkook Kim − *Multifunctional Nano Bio Electronics Lab, School of Advanced Materials Science and Engineering, Sungkyunkwan University, Suwon 16419, Gyeonggi-do, South Korea*; orcid.org/0000-0003-1747-4539; Email: seonkuk@skku.edu

Authors

Pavan Pujar − *Multifunctional Nano Bio Electronics Lab, School of Advanced Materials Science and Engineering, Sungkyunkwan University, Suwon 16419, Gyeonggi-do, South Korea*

Kishor Kumar Madaravalli Jagadeeshkumar − *Soft Materials Research Lab, Department of Chemical Engineering, National Institute of Technology Karnataka, Surathkal, India*

Muhammad Naqi − *Multifunctional Nano Bio Electronics Lab, School of Advanced Materials Science and Engineering, Sungkyunkwan University, Suwon 16419, Gyeonggi-do, South Korea*

Srinivas Gandla − *Multifunctional Nano Bio Electronics Lab, School of Advanced Materials Science and Engineering,*

https://dx.doi.org/10.1021/acsami.0c11193
ACS Appl. Mater. Interfaces XXXX, XXX, XXX−XXX

Sungkyunkwan University, Suwon 16419, Gyeonggi-do, South Korea; orcid.org/0000-0002-4586-1483

Hae Won Cho − *Multifunctional Nano Bio Electronics Lab, School of Advanced Materials Science and Engineering, Sungkyunkwan University, Suwon 16419, Gyeonggi-do, South Korea*

Sung Hyeon Jung − *School of Advanced Materials Science and Engineering, Sungkyunkwan University, Suwon, Gyeonggi-do 16419, Republic of Korea*

Hyung Koun Cho − *School of Advanced Materials Science and Engineering, Sungkyunkwan University, Suwon, Gyeonggi-do 16419, Republic of Korea;* orcid.org/0000-0003-0861-523X

Complete contact information is available at: https://pubs.acs.org/10.1021/acsami.0c11193

Author Contributions

‖P.P., K.K.M.J., and M.N. contributed equally to this work.

Notes

The authors declare no competing financial interest.

■ ACKNOWLEDGMENTS

The authors are thankful for support from the National Research Foundation of Korea (2018R1A2B2003558, 2018R1D1A1B07048232). The authors are grateful to Mainak Dutta for valuable inputs.

■ REFERENCES

(1) Yu, X.; Marks, T. J.; Facchetti, A. Metal Oxides for Optoelectronic Applications. *Nat. Mater* **2016**, *15*, 383−396.

(2) Coll, M.; Fontcuberta, J.; Althammer, M.; Bibes, M.; Boschker, H.; Calleja, A.; Cheng, G.; Cuoco, M.; Dittmann, R.; Dkhil, B.; El Baggari, I.; Fanciulli, M.; Fina, I.; Fortunato, E.; Frontera, C.; Fujita, S.; Garcia, V.; Goennenwein, S. T. B.; Granqvist, C.-G.; Grollier, J.; Gross, R.; Hagfeldt, A.; Herranz, G.; Hono, K.; Houwman, E.; Huijben, M.; Kalaboukhov, A.; Keeble, D. J.; Koster, G.; Kourkoutis, L. F.; Levy, J.; Lira-Cantu, M.; MacManus-Driscoll, J. L.; Mannhart, J.; Martins, R.; Menzel, S.; Mikolajick, T.; Napari, M.; Nguyen, M. D.; Niklasson, G.; Paillard, C.; Panigrahi, S.; Rijnders, G.; Sánchez, F.; Sanchis, P.; Sanna, S.; Schlom, D. G.; Schroeder, U.; Shen, K. M.; Siemon, A.; Spreitzer, M.; Sukegawa, H.; Tamayo, R.; Van Den Brink, J.; Pryds, N.; Granozio, F. M. Towards Oxide Electronics: A Roadmap. *Appl. Surf. Sci.* **2019**, *482*, 1−93.

(3) Pasquarelli, R. M.; Ginley, D. S.; O'Hayre, R. Solution Processing of Transparent Conductors: from flask to film. *Chem. Soc. Rev.* **2011**, *40*, 5406−5441.

(4) Talapin, D. V.; Lee, J.-S.; Kovalenko, M. V.; Shevchenko, E. V. Prospects of Colloidal Nanocrystals for Electronic and Optoelectronic Applications. *Chem. Rev.* **2009**, *110*, 389−458.

(5) Cochran, E. A.; Woods, K. N.; Johnson, D. W.; Page, C. J.; Boettcher, S. W. Unique Chemistries of Metal-Nitrate Precursors to Form Metal-Oxide Thin Films from Solution: Materials for Electronic and Energy Applications. *J. Mater. Chem. A* **2019**, *7*, 24124−24149.

(6) Mitzi, D. *Solution Processing of Inorganic Materials*; John Wiley & Sons, 2008.

(7) Bretos, I.; Jiménez, R.; Ricote, J.; Calzada, M. L. Low-Temperature Crystallization of Solution-derived Metal Oxide Thin Films Assisted by Chemical Processes. *Chem. Soc. Rev* **2018**, *47*, 291−308.

(8) Calzada, M. L. Sol−Gel Electroceramic Thin Films. In *The Sol−Gel Handbook*; Levy, D., Zayat, M., Eds.; John Wiley & Sons, 2015; pp 841−882.

(9) Schwartz, R. W.; Schneller, T.; Waser, R. Chemical Solution Deposition of Electronic Oxide Films. *C. R. Chim.* **2004**, *7*, 433−461.

(10) Banger, K. K.; Yamashita, Y.; Mori, K.; Peterson, R. L.; Leedham, T.; Rickard, J.; Sirringhaus, H. Low-Temperature, High-Performance Solution-Processed Metal Oxide Thin-Film Transistors Formed by a 'Sol−Gel on Chip' Process. *Nat. Mater.* **2011**, *10*, 45−50.

(11) Kim, M.-G.; Kanatzidis, M. G.; Facchetti, A.; Marks, T. J. Low-Temperature Fabrication of High-Performance Metal Oxide Thin-Film Electronics via Combustion Processing. *Nat. Mater.* **2011**, *10*, 382−388.

(12) Pujar, P.; Gandla, S.; Singh, M.; Gupta, B.; Tarafder, K.; Gupta, D.; Noh, Y.-Y.; Mandal, S. Development of Low Temperature Stoichiometric Solution Combustion Derived Transparent Conductive Ternary Zinc Tin Co-doped Indium Oxide Electrodes. *RSC Adv.* **2017**, *7*, 48253−48262.

(13) Kim, Y.-H.; Heo, J.-S.; Kim, T.-H.; Park, S.; Yoon, M.-H.; Kim, J.; Oh, M. S.; Yi, G.-R.; Noh, Y.-Y.; Park, S. K. Flexible Metal-Oxide Devices made by Room-Temperature Photochemical Activation of Sol−Gel Films. *Nature* **2012**, *489*, 128−132.

(14) Branquinho, R.; Salgueiro, D.; Santos, L.; Barquinha, P.; Pereira, L.; Martins, R.; Fortunato, E. Aqueous Combustion Synthesis of Aluminum Oxide Thin Films and Application as Gate Dielectric in GZTO Solution-Based TFTs. *ACS Appl. Mater. Interfaces* **2014**, *6*, 19592−19599.

(15) Liu, A.; Liu, G. X.; Zhu, H. H.; Xu, F.; Fortunato, E.; Martins, R.; Shan, F. K. Fully Solution-Processed Low-Voltage Aqueous In_2O_3 Thin-Film Transistors Using an Ultrathin ZrOx Dielectric. *ACS Appl. Mater. Interfaces* **2014**, *6*, 17364−17369.

(16) Sánchez, C.; Rozes, L.; Ribot, F.; Laberty-Robert, C.; Grosso, D.; Sassoye, C.; Boissiere, C.; Nicole, L. "Chimie douce": A Land of Opportunities for the Designed Construction of Functional Inorganic and Hybrid Organic-Inorganic Nanomaterials. *C. R. Chim.* **2010**, *13*, 3−39.

(17) Sassoye, Q. X.; McCleskey, T. M.; Burrell, A. K.; Lin, Y.; Collis, G. E.; Wang, H.; Li, A. D. Q.; Foltyn, S. R. Polymer-Assisted Deposition of Metal-Oxide Films. *Nat. Mater.* **2004**, *3*, 529−532.

(18) Zou, G. F.; Zhao, J.; Luo, H. M.; McCleskey, T. M.; Burrell, A. K.; Jia, Q. X. Polymer-Assisted-Deposition: A Chemical Solution Route for a Wide Range of Materials. *Chem. Soc. Rev.* **2013**, *42*, 439−449.

(19) Dai, X.; Deng, Y.; Peng, X.; Jin, Y. Quantum-Dot Light-Emitting Diodes for Large-Area Displays: Towards the Dawn of Commercialization. *Adv. Mater.* **2017**, *29*, 1607022.

(20) Bang, J. H.; Suslick, K. S. Applications of Ultrasound to the Synthesis of Nanostructured Materials. *Adv. Mater.* **2010**, *22*, 1039−1059.

(21) Doktycz, S.; Suslick, K. Interparticle Collisions Driven by Ultrasound. *Science* **1990**, *247*, 1067−1069.

(22) Suslick, K. S.; Hammerton, D. A.; Cline, R. E. The Sonochemical Hot Spot. *J. Am. Chem. Soc.* **1986**, *108*, 5641−5642.

(23) Woods, K. N.; Chiang, T.-H.; Plassmeyer, P. N.; Kast, M. G.; Lygo, A. C.; Grealish, A. K.; Boettcher, S. W.; Page, C. J. High-κ Lanthanum Zirconium Oxide Thin Film Dielectrics from Aqueous Solution Precursors. *ACS Appl. Mater. Interfaces* **2017**, *9*, 10897−10903.

(24) Liu, A.; Zhu, H.; Sun, H.; Xu, Y.; Noh, Y.-Y. Solution Processed Metal Oxide High-κ Dielectrics for Emerging Transistors and Circuits. *Adv. Mater.* **2018**, *30*, 1706364.

(25) Zhu, C.; Liu, A.; Liu, G.; Jiang, G.; Meng, Y.; Fortunato, E.; Martins, R.; Shan, F. Low-Temperature, Nontoxic Water-Induced High-κ Zirconium Oxide Dielectrics for Low-Voltage, High-Performance Oxide Thin-Film Transistors. *J. Mater. Chem. C* **2016**, *4*, 10715−10721.

(26) Fabrichnaya, O.; Lakiza, S.; Wang, C.; Zinkevich, M.; Aldinger, F. Assessment of Thermodynamic Functions in the ZrO_2−La_2O_3−Al_2O_3 System. *J. Alloys Compd.* **2008**, *453*, 271−281.

(27) Nicolosi, V.; Chhowalla, M.; Kanatzidis, M. G.; Strano, M. S.; Coleman, J. N. Liquid Exfoliation of Layered Materials. *Science* **2013**, *340*, 1226419.

(28) Kinsler, L.; Frey, A.; Coppens, A.; Sanders, J. *Fundamentals of Acoustics*, 3rd ed.; John Wiley & Sons, 1982.
(29) Maris, H.; Balibar, S. Negative Pressures and Cavitation in Liquid Helium. *Phys. Today* **2000**, *53*, 29−34.
(30) Suslick, K. S.; Flannigan, D. J. Inside a Collapsing Bubble: Sonoluminescence and the Conditions during Cavitation. *Annu. Rev. Phys. Chem.* **2008**, *59*, 659−683.
(31) Henglein, A.; Herburger, D.; Gutierrez, M. Sonochemistry: Some Factors that determine the Ability of a Liquid to Cavitate in an Ultrasonic Field. *J. Phys. Chem.* **1992**, *96*, 1126−1130.
(32) Hallmann, S.; Fink, M. J.; Mitchell, B. S. Mechanochemical Synthesis of Functionalized Silicon Nanoparticles with Terminal Chlorine Groups. *J. Mater. Res.* **2011**, *26*, 1052−1060.
(33) Gedanken, A. Using Sonochemistry for the Fabrication of Nanomaterials. *Ultrason. Sonochem.* **2004**, *11*, 47−55.

https://dx.doi.org/10.1021/acsami.0c11193
ACS Appl. Mater. Interfaces XXXX, XXX, XXX−XXX